Halloysite Nanotubes Functionalization with Phosphonic Acids: Role of Surface Charge on Molecule Localization and Reversibility

Tommaso Taroni[a,b], Daniela Meroni[a,b,*], Katarzyna Fidecka[a], Daniela Maggioni[a,b], Mariangela Longhi[a,b] and Silvia Ardizzone[a,b]

[a] *Chemistry Department, Università degli Studi di Milano, Via Golgi 19, 20133 Milan, Italy*

[b] *Consorzio INSTM, Via G. Giusti, 9, 50121, Florence, Italy*

* *Corresponding author: daniela.meroni@unimi.it*

Abstract

Halloysite nanotubes (HNT) are aluminosilicates bearing an Al-OH terminated inner lumen and a Si-O-Si exposing outer surface, which hold promise in several research fields due to their intrinsic surface duality. Functionalization with octylphophonic acid (OPA) was here investigated as a means to achieve selective functionalization of the HNT lumen and pH-triggered release. Model oxides were adopted to investigate the role of chemical nature and surface charge on the adsorption mode and reversibility of the OPA bond to the surface. Beside silica and aluminium (oxo)hydroxide used to mimic respectively the outer and inner HNT surfaces, titanium dioxide was also studied due to its intermediate isoelectric point and surface acidity. The effect of the functionalization pH and OPA content, along with the pH-dependent adsorption reversibility, were investigated using both spectroscopic characterization and wetting determinations. Results on both model oxides and HNT support a preferential adsorption of OPA on the Al-OH exposing surface. Functionalized HNT retained their inner lumen porosity and water dispersibility, which are desired properties in terms of application. The specific character of the OPA-HNT interaction is discussed with respect to (oxo)hydroxides, particularly in terms of the pH-dependent adsorption reversibility.

Keywords

Halloysite; phosphonate; oxide; functionalization; selective; surface

1. Introduction

Halloysite (HNT) is an aluminosilicate clay, which naturally comes in the form of nanotubes. Mainly extracted from mines in China, Australia, Mexico and Brazil, it is a hydrated polymorph of kaolinite, bearing the raw formula $Al_2(OH)_4Si_2O_5 \cdot nH_2O$ [1]. As in kaolin, layers of SiO_4 tetrahedra and AlO_6 octahedra constitute the crystalline lattice, but in halloysite the mismatch between the larger tetrahedral sheets and the smaller octahedral ones causes atomic-scale stress. Structural strain is solved by interstitial water molecules that force kaolin sheets to wrap and assume a tubular shape in which the inner and outer surfaces differ from each other [2]. The latter mainly exposes siloxane groups (Si-O-Si), even though silanol groups (Si-OH) are present as structural defects; the inner side presents instead aluminium hydroxide groups (Al-OH), showing different hydroxyl types (interlayer and inner surface) [2]. Both surfaces, when immersed in water between pH 2 and 8, are charged: the external surface bears a negative charge, while the inner lumen is positively charged, resulting in a net negative ζ-potential [3].

Owing to their low cost, availability and versatility, halloysite nanotubes offer prospects for a wealth of applications, including functional coatings, polymer nanocomposites, catalyst supports, adsorbents, and drug delivery [1,2]. The HNT fairly unique structural ambivalence is a powerful tool that might enable to modify separately the inner and outer surfaces, assigning them different tasks: in nanomedicine, theragnostic applications could be envisioned, coupling transport of active molecules [4–7] and diagnostics via triggered luminescent probes [8]; in nanocomposites and functional coatings, the outer surface of HNT could be modified to enhance compatibility with the matrix, while the inner lumen could be loaded with functional compounds (*e.g.*, eliciting anti-microbial or self-healing properties). Nonetheless, selective functionalization of halloysite nanotubes via covalent linkers is scarcely investigated in the literature, as precisely defining the nature and location of molecule adsorption is a complex matter. To help clarify this issue, in this work surface modification of halloysite was carried out together with the functionalization of purposely prepared model oxides mimicking the inner and outer surfaces.

To this task, phosphonic acids were chosen as functionalizing agents: they are hetero-organic compounds bearing a C-$PO(OH)_2$ group, which are known for adsorbing covalently on oxide substrates and can be used to create self-assembled monolayers [9,10]. Contrary to organosilanes, they do not suffer from homocondensation and their selectivity towards certain oxides [11] can be exploited for the selective functionalization of inherently dual systems, such as halloysite nanotubes. Although the literature reports several examples illustrating phosphonates inability to graft onto SiO_2 substrates in aqueous conditions [12,13], little is known about the real mechanism behind this behaviour. Various reports simply ascribe it to a generic susceptibility of Si-O-P bonds

to hydrolysis [14–18], while some suggest that in humid conditions a network of hydroxyls renders the SiO_2 surface unreactive [19].

Although a few literature studies report the modification of halloysite nanotubes with phosphonates, most of them simply use phosphonic acids as a surface modification strategy [20] without investigating the nature of the bond or its location. To date, the seminal paper by Yah *et al.* [21] remains the only paper investigating the location and adsorption mode of alkylphosphonic acids on halloysite nanotubes. However, the role of surface charge on the adsorption mechanism and the reversibility of the bond were not investigated in that paper and, to the authors' best knowledge, no previous reports on these issues can be found in the literature. For this reason, in our work particular attention was devoted to understanding the adsorption nature and gauging its reversibility, focusing on the role of the substrate surface charge. To this end, model oxides were also adopted, silica and alumina (oxo)hydroxide powders, mimicking the outer and inner surfaces of HNT, respectively. Octylphosphonic acid (OPA) was selected as functionalizing agent since its alkyl chain made it possible to monitor surface modification both by FTIR spectroscopy and macroscopical changes in surface properties, such as wetting and dispersibility. The role of different adsorption parameters was investigated, such as OPA concentration, reaction time and solution pH, while also checking adsorption reversibility.

2. Materials and methods

Halloysite nanotubes and chemicals were acquired from Sigma-Aldrich (unless differently stated) and were used without further purification; water was doubly distilled and deionised through a Milli-Q apparatus.

2.1 Preparation of model oxides

The adsorption of phosphonic acids at the surface of model oxides was investigated using silica and aluminium (oxo)hydroxide as models of the outer and inner surfaces of HNTs, respectively. In order to ensure the general validity of the results, both in-home synthesized and commercial oxides (SiO_2 from Sigma-Aldrich, AlO(OH) from Sasol) were adopted; the latter samples are identified in the text with a "c_" prefix. In order to better understand the effect of surface charge on the functionalization mechanism, in-home synthesized TiO_2 particles were also used for comparison in surface charge studies. Owing to the TiO_2 intermediate isoelectric point with respect to the other investigated oxides, the effect of a positive or negative surface charge on the adsorption mechanism could be evaluated by simply changing the functionalization pH in the 4-9 range, while keeping constant the oxide nature and morphology.

SiO_2 particles were prepared via a modified Stöber synthesis [22] using the following procedure: 5 mL of tetraethyl orthosilicate (TEOS), 75 mL of 99.8% ethanol and 10 mL of ammonium hydroxide (NH_4OH, 25%) were mixed, agitated for 30 s and then kept at room temperature for 4 h. The condensed phase was retrieved and washed nine times by centrifugation-resuspension cycles with distilled water, reaching neutral pH, after which it was dried at 70 °C for 24 h.

$Al(OH)_3$ particles were synthesized by forced hydrolysis, adapting the procedure reported by Kang *et al.* [23]. $Al(NO_3)_3 \cdot 9\ H_2O$ (2.2 mmol) and $Al_2(SO_4)_3 \cdot 16\ H_2O$ (0.32 mmol) were added to 280 mL of 0.1 M urea aqueous solution. The solution was kept at 98 °C without stirring for 4 h, during which a white solid started flocculating. Finally, the suspension was cooled to stop the reaction and the condensed phase was collected. The product was washed five times with water via centrifugation-resuspension cycles and dried at 100 °C for 24 h.

Finally, TiO_2 nanoparticles were prepared by a sol–gel synthesis according to a procedure previously reported by us [24]. Briefly, a solution of $Ti(OC_3H_7)_4$ in 2-propanol was hydrolysed at 65 °C by addition of water, adopting a water/alkoxide molar ratio of 100 and a water/2-propanol molar ratio of 20. The obtained precipitate was dried overnight at 90 °C, and then thermally treated at 300 °C for 5 h under O_2 stream.

2.2 Optimization of surface functionalization conditions

Surface functionalization of model oxides was conducted as follows. The oxide powder (200 mg) was suspended in 16 mL of a 1:1 water/2-propanol mixture and conditioned via sonication for 5 min. After the addition of the required amount of OPA, the suspension was stirred at room temperature (unless differently stated) for 1 h. For selected samples, the effect of functionalization temperature on adsorption was investigated in the range 0-80 °C. Longer functionalization times (up to 7 h) did not result in any significant improvement in the functionalization degree. The pH was monitored through a pH meter and adjusted at a value of either 4 or 9 with KOH and HNO_3 0.05 M solutions. Then, the powder was collected via centrifugation and dried at 100 °C for 24 h. Control tests were carried out washing the powder with a hydroalcoholic solution via centrifugation/resuspension cycles, giving fully comparable results. Functionalized samples bear the suffix –OPA.

For the sake of comparability among different oxides, nominal OPA amount was considered as surface density δ (*i.e.,* number of OPA molecules per nm^2), calculated according to the following equation:

$$\delta \equiv \frac{molecules_{OPA}}{nm^2_{sub}} = \frac{m_{OPA}}{MW_{OPA}} \cdot \frac{1}{SSA_{sub} \cdot m_{sub}} \cdot \frac{6.022 \times 10^{23}}{(10^9)^2}$$

where m_{OPA} and m_{sub} are respectively the amounts of OPA and of substrate expressed in g, MW_{OPA} is the molecular weight of OPA (in mol g^{-1}) and SSA_{sub} is the specific surface area of the oxide substrate expressed in $m^2 g^{-1}$. OPA surface density for each substrate was varied in the range 0.1-10 molecules nm^{-2}.

Functionalization of HNT was carried out according to a slightly modified procedure, in order to take into account their tubular morphology. The adopted HNT were purchased from Sigma-Aldrich and used without further purification; their main morphological and structural characteristics are reported in Tab. S1 and Figure S1; nanotubes present a broad size distribution and a noticeable degree of structural defectivity. 250 mg of HNT was added under stirring to a hydroalcoholic solution (4:1 ethanol/water mixture) of OPA (4 mM). The suspension was adjusted to pH 4, then it was transferred to a vacuum jar and evacuated using a vacuum pump. The fizzing of the suspension indicated that air was being removed from the HNT lumen and replaced with the OPA solution. The process of air evacuation and cycling back to atmospheric pressure was repeated three times, according to a procedure reported by Lvov *et al.* [21], in order to maximize OPA loading in the halloysite lumen. After stirring for a week at room temperature, the modified HNT was rinsed and centrifuged five times with a 4:1 ethanol/water mixture; it was then dried at 100 °C under vacuum for 24 h. The final product was labelled HNT-OPA.

2.3 Reversibility tests

Tests to assess the reversibility of the OPA adsorption were carried out on oxides previously functionalized at pH 4. Powders were dispersed via sonication in water, adjusting the pH at different values (either pH 4, 7 or 10) using diluted KOH and HNO_3 solutions, and stirred for 1 h. In the case of HNT, three vacuum cycles were also carried out in order to ensure solution access to the inner lumen. Then, the powders were collected by centrifugation and washed with 2-propanol to remove desorbed OPA residues. The recovered powders were then dried in oven at 70 °C.

2.4 Sample characterizations

The specific surface area of the samples was determined by means of N_2 adsorption-desorption isotherms in subcritical conditions recorded on a Coulter SA 3100 apparatus and analyzed according to the Brunauer–Emmett-Teller (BET) method. Desorption isotherms were used to determine the pore size distribution using the Barrett, Joyner, and Halenda (BJH) method.

X-ray diffraction (XRD) patterns of the powders were acquired at room temperature using a Siemens D5000 diffractometer equipped with a Cu Kα source (λ = 0.15406 nm), working at 40 kV

x 40 mA nominal X-rays power. θ : 2θ scans were performed between 10º and 80º, with step size 0.02º wide.

The isoelectric point (pH_{IEP}) was evaluated determining the oxide ζ-potential on a range of pH values using a Zetasizer Nano ZS (Malvern Instruments), operating at λ = 633 nm with a solid state He-Ne laser at a scattering angle of 173° and using the dip-cell kit. For ζ-potential measurements, powders were suspended in a 0.01 m KNO_3 aqueous solution, while pH was adjusted with diluted KOH and HNO_3 solutions. Average particle size determinations were performed on powder samples dispersed in milliQ water by dynamic light scattering (DLS) using the same instrument. Each hydrodynamic diameter as well as ζ-potential were averaged from at least three measurements.

Transmission electron microscopy (TEM) images were acquired using a Zeiss LEO 912ab Energy Filtering TEM operating at an acceleration voltage of 120 kV, equipped with a CCD-BM/1K system. Samples were dispersed in either 2-propanol or water (1 mg mL^{-1}) and deposited on Cu holey carbon grids (200 mesh).

Fourier transform infra-red (FTIR) spectra were registered using a Perkin Elmer Spectrum 100 spectrophotometer in Attenuated Total Reflectance (ATR) mode using a resolution of 4.0 cm^{-1} and acquiring 12 scans between 4000 and 400 cm^{-1}.

Dispersibility and suspension stability in water were assessed by measuring the absorbance at 550 nm of a 5 mg mL^{-1} HNT aqueous suspension at spontaneous pH as a function of time, using a Shimadzu UV2600 spectrophotometer.

Contact angle measurements, θ, were performed on oxide films, prepared by drop casting 1 mg mL^{-1} 2-propanol suspensions on glass, using a Krüss EasyDrop instrument. For each film, five static angles were measured, using 2 μL droplets of water.

Energy-dispersive X-ray spectroscopy (EDX) analyses were carried out using a Hitachi ED3000 probe on a Hitachi TM1000 scanning electron microscope operating at 15 kV.

3. Results and discussion

3.1 Functionalization of model oxides

The functionalization of aluminium (oxo)hydroxides and silica powders with OPA was investigated as model of the inner and outer surfaces of HNT. The main characteristics of the adopted model oxides are summarized in Tab. S1. To investigate the role of the oxide nature, deeply different materials, both morphologically and structurally, were chosen. It is noteworthy that comparable results were obtained on both commercial and in-home synthesized samples, supporting a role of

the oxide nature irrespective of the specific sample morphological and structural properties. Hence, in the following, only the most relevant samples will be shown.

Surface modification was studied via FTIR spectroscopy and contact angle measurements. Data relative to functionalization carried out at pH 4 will be first presented. FTIR spectroscopy was adopted to preliminarily assess the presence of OPA on the oxide surface upon functionalization. Figure 1 presents a comparison among the FTIR spectra of pristine and OPA-functionalized SiO_2 and $Al(OH)_3$, more specifically the region between 3200 and 2600 cm^{-1}, typical of aliphatic CH_x stretching. The relative spectra of the TiO_2 reference are reported in Figure S2.

After functionalization, both oxides display the characteristic stretching signals of aliphatic chains at 2959, 2925 and 2854 cm^{-1}, belonging to the asymmetrical modes of methyl groups, and the asymmetrical and symmetrical modes of methylene, respectively [25]; the position of the CH_x stretching bands supports a disordered orientation of the alkyl chains [26]. Notwithstanding the difference in specific surface area between the two oxides, the alkyl chains peaks are more appreciable in the case of $Al(OH)_3$, especially in the spectra of δ_7 and δ_{10} samples. The TiO_2 spectra show a trend similar to $Al(OH)_3$ samples.

Contact angle measurement is one of the most commonly adopted techniques to assess the quality of surface modification [27], as the wetting properties of the support may drastically change after the functionalization. The functionalization effect on the surface wettability was investigated by monitoring the contact angle as a function of the phosphonic acid amount. In Figure 2, the average water contact angles of $Al(OH)_3$ and SiO_2 films are plotted against the nominal surface density of OPA molecules and compared with those of TiO_2 films as reference. All of the pristine oxides show a complete water spreading. However, upon functionalization, largely different trends are appreciable among the investigated oxides: as the OPA amount increases, the contact angle of the functionalized $Al(OH)_3$ grows up to around 135° at *ca.* 4 molecules nm^{-2}; conversely, the wettability of functionalized SiO_2 is hardly affected and sits around 0°. However, when using CH_2I_2 instead of water, the measured contact angles increased with the nominal OPA amount in a rather similar way for each oxide, as can be seen in Figure S3. This observation is in agreement with FTIR spectra showing the presence of OPA molecules also on the SiO_2 surface.

These results suggest that OPA molecules on alumina (oxo)hydroxide substrates orient their polar heads towards the surface, exposing the hydrophobic alkyl chains, whereas on silica the phosphonic head forms labile interactions with the oxide and as a result, molecules are solubilised by the probe polar solvent, *i.e.* water.

Figure 3 reports the differential FTIR spectra for the three oxides in the region between 1500 and 800 cm^{-1}, typical of the phosphonate head signals. All oxides present a band at *ca.* 1460 cm^{-1} which

can be attributed to the scissoring mode of CH_2 [28]. Functionalized SiO_2 samples show no signal but those relative to free phosphonate P-O stretching and P-O-H bending at 1000 and 950 cm^{-1}, respectively [29], confirming the lack of Si-O-P bonds which should be instead appreciable at ca. 1080 cm^{-1} [30]. Alumina hydroxide spectra show no free P=O stretching band at 1220 cm^{-1}, indicative of unbound OPA molecules, although a slight signal at 1220 cm^{-1} becomes appreciable only when a surface coverage plateau is reached (as observed in terms of contact angle). Moreover, the $Al(OH)_3$ spectra present a broad band centred at 1050 cm^{-1}, which could be the convolution of several components. In this respect, the AlO(OH) spectra (Figure S4) show sharper peaks in this region: a main component at 1070 cm^{-1}, a second peak at 1150 cm^{-1} and a shoulder at 1000 cm^{-1}, which can be attributed to stretching modes of Al-O-P, bound P=O and P-O, respectively. It should be noted that these three components show an appreciable shift to lower frequencies at increasing OPA contents. On the other hand, TiO_2 shows a different behaviour: at lower surface densities, both free and bound P=O signals can be appreciated at 1220 and 1150 cm^{-1} respectively, together with the bands at 1070 and 1000 cm^{-1}, relative to Ti-O-P moieties and free P-O [31]. When surface coverage increases, the peak at 1220 cm^{-1} disappears, while the three components at 1150, 1070 and 1000 cm^{-1} merge into a single broad band. These observations can be explained on the grounds of the different Lewis acidity of aluminium (oxo)hydroxide and TiO_2, which affects OPA coordination: in the case of Lewis acidic metal oxides such as aluminium (oxo)hydroxide, OPA will adsorb on the surface coordinating its P=O moiety first and then will form Al-O-P bonds with its P-OH groups. Conversely, in the case of poor Lewis acids nucleophilic M-OH groups attack the P centre, leading then to surface binding with a minor contribution of P=O [29,32]. TiO_2 being a poorer Lewis acid compared to aluminium (oxo)hydroxides, the OPA molecule coordination appears to fall in between the two descriptions, as supported by the presence of both types of P=O signals.

The effect of temperature on adsorption was tested in the 0-80°C range. No significant differences are appreciable both in terms of contact angle and FTIR spectra (Figure S5). In the adopted functionalization conditions, temperature does not seem to play a key role. Moreover, FTIR spectra exhibit similar features across the investigated temperature range (Fig. S5 B), suggesting a levelling effect introduced by the final thermal treatment.

To better understand the nature of adsorbent-adsorbate interaction, the role of the pH of functionalization was investigated with respect to the surface charge of each oxide and of the speciation of the functionalizing agent. To this aim, functionalization tests were conducted at either pH 4 or 9. The relative contact angle isotherms are reported in Figure 4.

While for both SiO_2 (not shown) and $Al(OH)_3$ increasing the functionalization pH has a negligible effect, in the case of TiO_2 the impact was visible, especially for lower OPA amounts, and hydrophobic plateau could not be reached even at higher OPA densities. The observed difference in behaviour between oxides can be rationalized on the grounds of their surface charge properties, in particular of their pH_{IEP} values. Figure 5 reports the ζ-potential curves used for isoelectric point determinations. The measured pH_{IEP} values, reported in the inset table, are in good agreement with literature data [33].

According to pH_{IEP} values, SiO_2 is negatively charged at both the investigated functionalization pH values, whereas $Al(OH)_3$ is positively charged at both pH values. Conversely, the surface charge of TiO_2 was positively charged at pH 4 and negatively charged at pH 9. Considering that the pK_{a1} and pK_{a2} of OPA are respectively at 2.7 and 8.2 [34], the OPA molecule is negatively charged due to deprotonation at both the investigated pH values, more so at pH 9. We can thus conclude that electrostatic repulsion played a fundamental role in determining the susceptibility to hydrolysis of the M-O-P bond, which was enhanced by negative surface charge, as it will be more extensively discussed in Section 3.3.

3.2 Characterization of HNT-OPA

Figure 6 reports the FTIR spectra of HNT before and after functionalization with OPA, in the frequency region between 2800 and 3800 cm^{-1}, characteristic of OH and CH_x stretching signals, where the main changes are appreciable.

The untreated HNT shows three main signals: peaks at 3692 and 3622 cm^{-1} can be attributed to the stretching of inner and interlayer Al-μ_2-OH groups respectively [35], while the band at 3548 cm^{-1} can be assigned to the stretching of the hydrogen bonded OH groups of intercalated water [36]. Beneath these sharper peaks, the broad band of O-H stretching, due to physisorbed water, extends from 3750 cm^{-1} to 3000 cm^{-1}. After the functionalization, a general intensity decrease is observed in the O-H stretching region: this might be related to a loss of surface hydroxyls [37]. Moreover, the appearance of the characteristic CH_x stretching bands at 2956, 2926 and 2853 cm^{-1}, confirmed the presence of disordered OPA aliphatic chains [25]. Figure S6 compares the FTIR spectra of HNT and HNT-OPA in the 1500-800 cm^{-1} region, along with their differential spectrum. Beside the CH_2 deformation band at 1460 cm^{-1}, other signals attributable to OPA are present. The two bands at 1203 and 1156 cm^{-1} might be due to free and bound P=O stretching, while the sharp peak at 1083 cm^{-1} could be attributed to Al-O-P stretching. A small peak at 985 cm^{-1} is noticeable. The occurrence of both free and bound P=O stretching supports the ^{31}P solid state NMR findings reported by Yah and coauthors [21] suggesting the copresence of bi- and tridentate binding modes.

Furthermore, the presence of the two different P=O components might suggest that the OPA-HNT mode of adsorption does not closely mirror the OPA-Al (oxo)hydroxide interactions shown in Figures 3a and S4. In this respect, the use of models allowed us to shed light onto the inherently complex P-O stretching region.

N_2 adsorption-desorption isotherms in subcritical conditions carried out on bare HNT yielded a specific surface area of 53 m^2 g^{-1}, in line with previously reported values [2]. After functionalization, the sample showed a 13% decrease in surface area (46 m^2 g^{-1}). Porosity also incurred in some changes: while the total pore volume did not decrease by a great margin (from 0.338 to 0.307 mL g^{-1}, about 9%), a notable loss of micropores is observed (Figure 7a). Similar results have been reported in the case of surface functionalization of oxides with organosilanes [24,38]. In the present case, the OPA molecules (*ca.* 1 nm in length) might clog the smaller pores. The small peak in the pore size distribution of the pristine material at around 20 nm can be related to the inner lumen of the nanotubes, as shown by TEM images (Figure 7b and Figure S1) reporting an inner lumen of 10-30 nm. By comparing the pore size distributions before and after OPA functionalization, it is clear that this peak is not affected by the presence of OPA, suggesting that the lumen is not occluded by organic matter. Conversely, Yah *et al.* [21] reported a much higher loss in specific surface area and a decrease in pore size relative to pores of *ca.* 25 nm; these differences can be explained by the much longer alkyl chain (18 C atoms against 8) of the phosphonic acid derivative used by Yah and co-authors, which hindered the inner lumen accessibility.

Figure 8 reports ζ-potential measurements of the pristine and functionalized HNT as a function of pH. The ζ-potential curves of HNT and HNT-OPA differ significantly for pH values higher than 2.5, the latter sample being more negatively charged. The two curves converge at lower pH values, resulting in the same pH_{IEP} of around 1.5, a typical value for HNT [39]. The difference between the two curves can be traced back to the presence of OPA on the inner surface of functionalized HNTs: the covalent binding of OPA removes Al-OH groups, which are responsible for the positive charge of the inner surface, similarly to what previously reported in the case of anionic surfactants [40]. Furthermore, above its pK_{a1} at 2.8, OPA is deprotonated and its negative charge sums up with the basal negative charge of HNT [1]. For pH value more acidic than 2.8, the OPA negative charge is neutralized by protonation and stops affecting HNT ζ-potential.

Water dispersibility and dispersion stability of the pristine and functionalized HNT were compared at spontaneous pH (*ca.* 4). Both samples presented fully comparable molar extinction coefficient at the selected wavelength (550 nm), hence differences in absorbance can be related to the actual dispersion concentration. Initial absorbance was 0.32 and 0.45 for HNT and HNT-OPA,

respectively. Figure 8b reports the samples normalized absorbance over time to compare the suspension stability. The functionalized HNT displayed a better dispersibility and suspension stability than the pristine sample. It should be noted that the model oxides functionalized with OPA present a much lower dispersibility in water than the bare analogue (particles float in aqueous solvent, Figure S7) due to the hydrophobic properties imparted by the OPA coating. The higher dispersibility of HNT-OPA suggests that no OPA was bound on the external SiO_2 surface, which thus retains its hydrophilic properties. The enhanced suspension stability can possibly be explained on the grounds of the higher negative charge of the functionalized sample, as reported by ζ-potential measurements, which may have contributed to increasing electrostatic repulsion between particles, enhancing their stability. Overall, our results are in good agreement with XPS evidence reported in the literature [21] showing no alteration of the Si peak upon alkyl phosphonic acid functionalization of halloysites.

3.3 Reversibility tests

The reversibility of OPA adsorption was investigated for both the model oxides and HNT, upon treatment in a range of pH values. To the authors' best knowledge, the reversibility of the bond of alkyl chain phosphonic acids on halloysite nanotubes has not been previously investigated in the literature. In this respect, it should be noted that, in the work by Yah and co-workers [21], release tests of ferrocene derivatives do not consider the reversibility of the phosphonic acid bond with the oxide, as the ferrocene compounds were merely physisorbed due to compatibility with the hydrophobic alkyl chains. Due to the previously discussed labile nature of the OPA adsorption on silica, results relative to SiO_2 samples are not presented in this section.

Figure 9 shows the effect of a release treatment at pH 10 on the wetting properties of various oxides. While all samples exhibited quite comparable wetting features (contact angles > 130°) upon OPA functionalization, notable differences are appreciable among the different oxides after treatment in alkaline environment. TiO_2 shows a complete water spreading upon treatment in alkaline conditions, which is indicative of a loss of OPA coverage. Aluminium (oxo)hydroxides show instead a more complex behaviour: $Al(OH)_3$ retains the surface functionalization upon treatment at pH 9, as shown by the water contact angle (Figure 9a,b) whereas c_AlO(OH) shows a marked loss in hydrophobicity upon treatment (Figure 9c,d), even though the surface does not recover the superhydrophilic properties of the pristine sample. These observations can be explained on the grounds of the pH_{IEP} of the substrate: TiO_2 suffers a drastic loss of OPA upon treatment at a pH value much higher than its isoelectric point (Fig. 4 inset), whereas in the case of $Al(OH)_3$, a treatment at the same pH value has hardly any effect thanks to the sample very alkaline pH_{IEP} (close

to 10). Notably, c_AlO(OH) shows an intermediate behaviour in terms of OPA release, due to its lower pH_{IEP} (9.0).

Table 1 reports water contact angles and P/metal ratios, determined by EDX, of functionalized samples before and after reversibility tests at different pH values (4, 7 or 10). EDX results compare well with the calculated OPA surface density, within the experimental limits of the technique. Surface wetting and the phosphorous content show comparable trends, confirming that the decrease in hydrophobicity is related to the loss of adsorbed OPA molecules. Results confirm the hypothesized trend based on the surface charge properties of each oxide: while treatment at pH 4 showed negligible effects in terms of both surface wetting and phosphor amount for all the investigated oxides, TiO_2 and aluminium (oxo)hydroxides powders treated at pH values higher than their pH_{IEP} highlighted a loss of OPA coverage. Interestingly, OPA loss is not complete upon treatment at pH values close or slightly higher than the pH_{IEP}, as shown by tests with TiO_2 at pH 7 and c_AlO(OH) at pH 10, which indicates that the OPA-oxide interaction is not merely based on electrostatic interactions, in agreement with FTIR results showing the occurrence of M-O-P bonds. Nonetheless, our results suggest that the initial driving force is mainly electrostatic and that surface charge plays a role also on the stability of the bond.

The case of HNT-OPA is more complex given that the measured isoelectric point is a global parameter that does not account for the different protonation equilibria of the two surfaces [39]. Despite the very acidic pH_{IEP} of HNT, treatment at pH 4 does not significantly reduce the OPA adsorption, whereas a drastic decrease in OPA content is appreciable for treatment in neutral and alkaline conditions. As reported by Bretti *et al.* [3,41], at pH 4 about half of the outer Si-OH sites and all of the inner Al-OH ones are protonated. When increasing the pH to 7 the whole SiO_2 surface is deprotonated, together with part of the inner surface. At pH 10 both surfaces are almost completely deprotonated. The present results can be rationalized considering that at neutral pH the effective HNT surface charge is negative enough to detach adsorbed OPA.

4. Conclusions

An in-depth understanding of molecule adsorption onto structurally complex materials, such as halloysite, is essential whenever fine tuning of surface features is sought after. Functionalization with phosphonic acids can provide a selective functionalization of the inner lumen of HNT, as shown in the present study by model oxides and complementary characterizations. Upon functionalization, HNT showed enhanced dispersibility in water as a result of the increased surface charge, proving this surface modification compatible with usage in aqueous conditions. Moreover, accessibility to the inner lumen, a key parameter for further loading of compounds, was retained.

Halloysite nanotubes are often adopted as smart delivery systems, *e.g.* for the loading and release of active compounds in nanocomposites and nanocarriers. These applications require the design of functional linkers enabling the triggered release of loaded compounds. In the present study, the reversibility of the OPA-HNT bond was investigated, showing a pH sensitive behaviour, dependent on the oxide surface charge. In this respect, oxide models proved crucial in understanding the relation between support and adsorbate, showing a key role of surface charge on the bond formation and stability. We purposely chose three model oxides bearing different surface electrification features to compare their behaviour. For example, tests performed on TiO_2 at pH 4 and 9 show a clear difference in adsorption and reversibility, due to the oxide opposite surface charge at the two pH values. This is not the case for $Al(OH)_3$, which is positively charged at both pH values and hence shows comparable behaviour in the two sets of tests. This comparison excludes the role of OPA protonation degree and suggests that it is instead the oxide specific electrification that influences adsorption. On the other hand, the interaction of halloysite nanotubes with OPA showed a peculiar character, in terms of adsorption mode and sensitivity to hydrolysis, arising from their complex structure.

The present results offer prospects for applications where a selective loading of the inner lumen and a pH-triggered release of active components are required. Moreover, the here proposed combined characterization approach could be applied to other functionalizing agents to clarify their localization and interaction with HNT.

References

[1] Y. Lvov, W. Wang, L. Zhang, R. Fakhrullin, Halloysite Clay Nanotubes for Loading and Sustained Release of Functional Compounds, Adv. Mater. 28 (2016) 1227–1250. doi:10.1002/adma.201502341.

[2] P. Yuan, D. Tan, F. Annabi-Bergaya, Properties and applications of halloysite nanotubes: recent research advances and future prospects, Appl. Clay Sci. 112–113 (2015) 75–93. doi:10.1016/j.clay.2015.05.001.

[3] C. Bretti, S. Cataldo, A. Gianguzza, G. Lando, G. Lazzara, A. Pettignano, S. Sammartano, Thermodynamics of Proton Binding of Halloysite Nanotubes, J. Phys. Chem. C. 120 (2016) 7849–7859. doi:10.1021/acs.jpcc.6b01127.

[4] J. Yang, Y. Wu, Y. Shen, C. Zhou, Y.F. Li, R.R. He, M. Liu, Enhanced Therapeutic Efficacy of Doxorubicin for Breast Cancer Using Chitosan Oligosaccharide-Modified Halloysite Nanotubes, ACS Appl. Mater. Interfaces. 8 (2016) 26578–26590.

doi:10.1021/acsami.6b09074.

[5] H. Lun, J. Ouyang, H. Yang, Natural halloysite nanotubes modified as an aspirin carrier, RSC Adv. 4 (2014) 44197–44202. doi:10.1039/C4RA09006C.

[6] Y.M. Lvov, M.M. DeVilliers, R.F. Fakhrullin, The application of halloysite tubule nanoclay in drug delivery, Expert Opin. Drug Deliv. 13 (2016) 977–986. doi:10.1517/17425247.2016.1169271.

[7] P. Yuan, P.D. Southon, Z. Liu, C.J. Kepert, Organosilane functionalization of halloysite nanotubes for enhanced loading and controlled release, Nanotechnology. 23 (2012) 375705. doi:10.1088/0957-4484/23/37/375705.

[8] H. Zhang, T. Ren, Y. Ji, L. Han, Y. Wu, H. Song, L. Bai, X. Ba, Selective Modification of Halloysite Nanotubes with 1-Pyrenylboronic Acid: A Novel Fluorescence Probe with Highly Selective and Sensitive Response to Hyperoxide, ACS Appl. Mater. Interfaces. 7 (2015) 23805–23811. doi:10.1021/acsami.5b08600.

[9] L. Sang, K.M. Knesting, A. Bulusu, A.K. Sigdel, A.J. Giordano, S.R. Marder, J.J. Berry, S. Graham, D.S. Ginger, J.E. Pemberton, Effect of time and deposition method on quality of phosphonic acid modifier self-assembled monolayers on indium zinc oxide, Appl. Surf. Sci. 389 (2016) 190–198. doi:10.1016/j.apsusc.2016.06.183.

[10] D.M. Spori, N. V. Venkataraman, S.G.P. Tosatti, F. Durmaz, N.D. Spencer, S. Zürcher, Influence of alkyl chain length on phosphate self-assembled monolayers, Langmuir. 23 (2007) 8053–8060. doi:10.1021/la700474v.

[11] S.P. Pujari, L. Scheres, A.T.M. Marcelis, H. Zuilhof, Covalent surface modification of oxide surfaces, Angew. Chemie - Int. Ed. 53 (2014) 6322–6356. doi:10.1002/anie.201306709.

[12] O. Acton, D. Hutchins, L. Árnadóttir, T. Weidner, N. Cernetic, G.G. Ting, T.W. Kim, D.G. Castner, H. Ma, A.K.Y. Jen, Spin-cast and patterned organophosphonate self-assembled monolayer dielectrics on metal-oxide-activated Si, Adv. Mater. 23 (2011) 1899–1902. doi:10.1002/adma.201004762.

[13] S. Lassiaz, D. Labarre, A. Galarneau, D. Brunel, P.H. Mutin, Modification of silica by an organic monolayer in aqueous medium using octylphosphonic acid and aluminium species, J. Mater. Chem. 21 (2011) 8199–8205. doi:10.1039/c1jm10128e.

[14] S.K. Davidowski, G.P. Holland, Solid-State NMR Characterization of Mixed Phosphonic Acid Ligand Binding and Organization on Silica Nanoparticles, Langmuir. 32 (2016) 3253–3261. doi:10.1021/acs.langmuir.5b03933.

[15] P.H. Mutin, V. Lafond, A.F. Popa, M. Granier, L. Markey, A. Dereux, Selective Surface Modification of SiO_2 $-TiO_2$ Supports with Phosphonic Acids, Chem. Mater. 16 (2004) 5670–

5675. doi:10.1021/cm035367s.

[16] R.J.P. Corriu, D. Leclercq, P.H. Mutin, L. Sarlin, A. Vioux, Nonhydrolytic sol-gel routes to layered metal(IV) and silicon phosphonates, J. Mater. Chem. 8 (1998) 1827–1833. doi:10.1039/a803755h.

[17] C. Weinberger, T. Heckel, P. Schnippering, M. Schmitz, A. Guo, W. Keil, H.C. Marsmann, C. Schmidt, M. Tiemann, R. Wilhelm, Straightforward Immobilization of Phosphonic Acids and Phosphoric Acid Esters on Mesoporous Silica and Their Application in an Asymmetric Aldol Reaction, Nanomaterials. 9 (2019) 249. doi:10.3390/nano9020249.

[18] F. Hoffmann, M. Cornelius, J. Morell, M. Fröba, Silica-Based Mesoporous Organic–Inorganic Hybrid Materials, Angew. Chemie Int. Ed. 45 (2006) 3216–3251. doi:10.1002/anie.200503075.

[19] A. Vega, P. Thissen, Y.J. Chabal, Environment-controlled tethering by aggregation and growth of phosphonic acid monolayers on silicon oxide, Langmuir. 28 (2012) 8046–8051. doi:10.1021/la300709n.

[20] H. Jing, Y. Higaki, W. Ma, H. Wu, W.O. Yah, H. Otsuka, Y.M. Lvov, A. Takahara, Internally Modified Halloysite Nanotubes as Inorganic Nanocontainers for a Flame Retardant, Chem. Lett. 42 (2013) 121–123. doi:10.1246/cl.2013.121.

[21] W.O. Yah, A. Takahara, Y.M. Lvov, Selective Modification of Halloysite Lumen with Octadecylphosphonic Acid: New Inorganic Tubular Micelle, J. Am. Chem. Soc. 134 (2012) 1853–1859. doi:10.1021/ja210258y.

[22] S.L. Greasley, S.J. Page, S. Sirovica, S. Chen, R.A. Martin, A. Riveiro, J. V. Hanna, A.E. Porter, J.R. Jones, Controlling particle size in the Stöber process and incorporation of calcium, J. Colloid Interface Sci. 469 (2016) 213–223. doi:10.1016/j.jcis.2016.01.065.

[23] B.K. Kang, H.D. Lim, S.R. Mang, K.M. Song, M.K. Jung, S.-W. Kim, D.H. Yoon, Synthesis and Characterization of Monodispersed β-Ga_2O_3 Nanospheres via Morphology Controlled Ga 4 (OH) 10 SO 4 Precursors, Langmuir. 31 (2015) 833–838. doi:10.1021/la504209f.

[24] F. Milanesi, G. Cappelletti, R. Annunziata, C.L. Bianchi, D. Meroni, S. Ardizzone, Siloxane-TiO_2 hybrid nanocomposites. the structure of the hydrophobic layer, J. Phys. Chem. C. 114 (2010) 8287–8293. doi:10.1021/jp1014669.

[25] R. Luschtinetz, G. Seifert, E. Jaehne, H.J.P. Adler, Infrared spectra of alkylphosphonic acid bound to aluminium surfaces, Macromol. Symp. 254 (2007) 248–253. doi:10.1002/masy.200750837.

[26] T. Vallant, J. Kattner, H. Brunner, U. Mayer, H. Hoffmann, Investigation of the formation and structure of self-assembled alkylsiloxane monolayers on silicon using in situ attenuated

total reflection infrared spectroscopy, Langmuir. 15 (1999) 5339–5346. doi:10.1021/la9900977.

[27] D. Meroni, S. Ardizzone, U.S. Schubert, S. Hoeppener, Probe-Based Electro-Oxidative Lithography of OTS SAMs Deposited onto Transparent ITO Substrates, Adv. Funct. Mater. 22 (2012) 4376–4382. doi:10.1002/adfm.201200673.

[28] S. Zorn, U. Dettinger, M.W.A. Skoda, R.M.J. Jacobs, H. Peisert, A. Gerlach, T. Chassé, F. Schreiber, Stability of hexa(ethylene glycol) SAMs towards the exposure to natural light and repeated reimmersion, Appl. Surf. Sci. 258 (2012) 7882–7888. doi:10.1016/j.apsusc.2012.04.110.

[29] P.J. Hotchkiss, S.C. Jones, S.A. Paniagua, A. Sharma, B. Kippelen, N.R. Armstrong, S.R. Marder, The modification of indium tin oxide with phosphonic acids: Mechanism of binding, tuning of surface properties, and potential for use in organic electronic applications, Acc. Chem. Res. 45 (2012) 337–346. doi:10.1021/ar200119g.

[30] P. Thissen, A. Vega, T. Peixoto, Y.J. Chabal, Controlled, Low-Coverage Metal Oxide Activation of Silicon for Organic Functionalization: Unraveling the Phosphonate Bond, (2012). doi:10.1021/la3038457.

[31] P. Kim, S.C. Jones, P.J. Hotchkiss, J.N. Haddock, B. Kippelen, S.R. Marder, J.W. Perry, Phosphonic acid-modified barium titanate polymer nanocomposites with high permittivity and dielectric strength, Adv. Mater. 19 (2007) 1001–1005. doi:10.1002/adma.200602422.

[32] F. Brodard-Severac, G. Guerrero, J. Maquet, P. Florian, C. Gervais, P.H. Mutin, High-field ^{17}O MAS NMR investigation of phosphonic acid monolayers on titania, Chem. Mater. 20 (2008) 5191–5196. doi:10.1021/cm8012683.

[33] M. Kosmulski, Isoelectric points and points of zero charge of metal (hydr)oxides: 50 years after Parks' review, Adv. Colloid Interface Sci. 238 (2016) 1–61. doi:10.1016/j.cis.2016.10.005.

[34] P.C. Crofts, G.M. Kosolapoff, Preparation and Determination of Apparent Dissociation Constants of Some Alkylphosphonic and Dialkylphosphinic Acids, J. Am. Chem. Soc. 75 (1953) 3379–3383. doi:10.1021/ja01110a024.

[35] E. Joussein, S. Petit, J. Churchman, B. Theng, D. Righi, B. Delvaux, Halloysite clay minerals – a review, Clay Miner. 40 (2005) 383–426. doi:10.1180/0009855054040180.

[36] B.K.G. Theng, Surface Properties of Allophane, Halloysite, and Imogolite, Clays Clay Miner. 30 (1982) 143–149. doi:10.1346/CCMN.1982.0300209.

[37] G. Soliveri, V. Pifferi, R. Annunziata, L. Rimoldi, V. Aina, G. Cerrato, L. Falciola, G. Cappelletti, D. Meroni, Alkylsilane-SiO_2 Hybrids. A Concerted Picture of Temperature

Effects in Vapor Phase Functionalization, J. Phys. Chem. C. 119 (2015) 15390–15400. doi:10.1021/acs.jpcc.5b04048.

[38] G. Soliveri, R. Annunziata, S. Ardizzone, G. Cappelletti, D. Meroni, Multiscale rough titania films with patterned hydrophobic/oleophobic features, J. Phys. Chem. C. 116 (2012) 26405–26413. doi:10.1021/jp309397c.

[39] G. Tarì, I. Bobos, C.S.F. Gomes, J.M.F. Ferreira, Modification of surface charge properties during kaolinite to halloysite-7Å transformation, J. Colloid Interface Sci. 210 (1999) 360–366. doi:10.1006/jcis.1998.5917.

[40] G. Cavallaro, G. Lazzara, S. Milioto, Exploiting the Colloidal Stability and Solubilization Ability of Clay Nanotubes/Ionic Surfactant Hybrid Nanomaterials, J. Phys. Chem. C. 116 (2012) 21932–21938. doi:10.1021/jp307961q.

[41] M. Massaro, G. Lazzara, S. Milioto, R. Noto, S. Riela, Covalently modified halloysite clay nanotubes: synthesis, properties, biological and medical applications, J. Mater. Chem. B. 5 (2017) 2867–2882. doi:10.1039/c7tb00316a.

Table 1 – Phosphor content (from EDX) and water contact angle values of OPA functionalized samples before and after treatment at various pH values. DL stands for detection limit.

sample	P/(Al,Ti) molar ratio / %			
	functionalized	after reversibility test		
		pH 4	pH 7	pH 10
$Al(OH)_3$-OPA δ_{10}	6.6 ± 0.6	7.8 ± 0.6	7.7 ± 0.7	6.4 ± 0.7
c_AlO(OH)-OPA δ_2	10.5 ± 0.3	10.2 ± 0.3	7.9 ± 0.8	5 ± 1
TiO_2 -OPA δ_2	1.8 ± 0.2	1.4 ± 0.2	1.2 ± 0.1	< DL
HNT-OPA	6 ± 1	7.3 ± 0.9	< DL	< DL

sample	water contact angle / °			
	functionalized	after reversibility test		
		pH 4	pH 7	pH 10
$Al(OH)_3$-OPA δ_{10}	149 ± 1	151 ± 2	152 ± 2	138 ± 3
c_AlO(OH)-OPA δ_2	134 ± 5	122 ± 3	120 ± 19	17 ± 2
TiO_2 -OPA δ_2	156 ± 4	148 ± 7	85 ± 22	< 5

Figure captions

Figure 1 – FTIR spectra of pristine and OPA-functionalized SiO_2 (A) and $Al(OH)_3$ (B); the functionalization was carried out at pH 4.

Figure 2 – Water contact angles of functionalized oxide films as a function of the nominal OPA surface coverage (functionalization at pH 4). Error bars are in the order of the markers size.

Figure 3 – Differential FTIR spectra of functionalized $Al(OH)_3$ (A), SiO_2 (B) and TiO_2 (C), obtained by subtracting the relative spectrum of the pristine oxide; functionalization was carried out at pH 4.

Figure 4 – Water average contact angle vs. OPA nominal surface density for $Al(OH)_3$ (A) and TiO_2 (B) impregnated either at pH 4 or 9.

Figure 5 – ζ-potential curves as a function of pH and the resulting pH_{IEP} values (inset) for pristine TiO_2, $Al(OH)_3$ and SiO_2.

Figure 6 – FTIR spectra of pristine and OPA-functionalized HNT.

Figure 7 – Pore size distribution of HNT before and after functionalization (a); TEM image of pristine HNT (b).

Figure 8 – ζ-potential curves before and after functionalization (A) and normalized absorbance (550 nm) of suspensions of pristine and OPA-functionalized HNT in water over time (B).

Figure 9 – Water contact angles on OPA-functionalized $Al(OH)_3$ (A, B), c_AlO(OH) (C, D) and TiO_2 (E, F) before and after release treatment at pH 10.

Figure
Click here to download Figure: revised Figures.docx

Figures

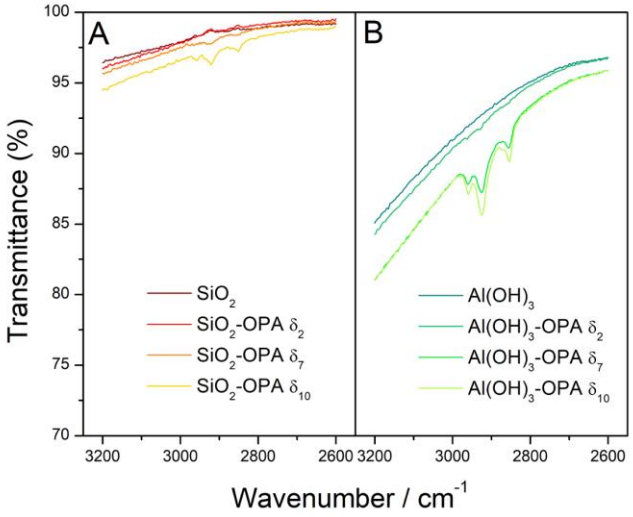

Figure 1

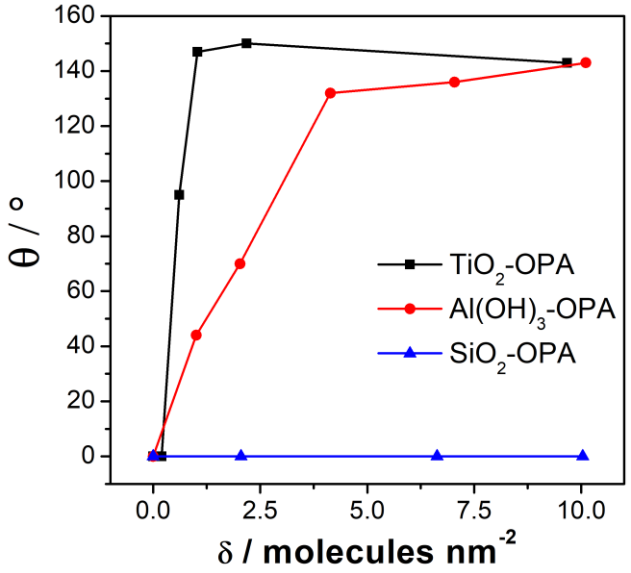
160
140
120
100
80
60
40
20
0
θ / °
0.0
2.5
5.0
7.5
10.0
δ / molecules nm-2
TiO2-OPA
Al(OH)3-OPA
SiO2-OPA

Figure 2

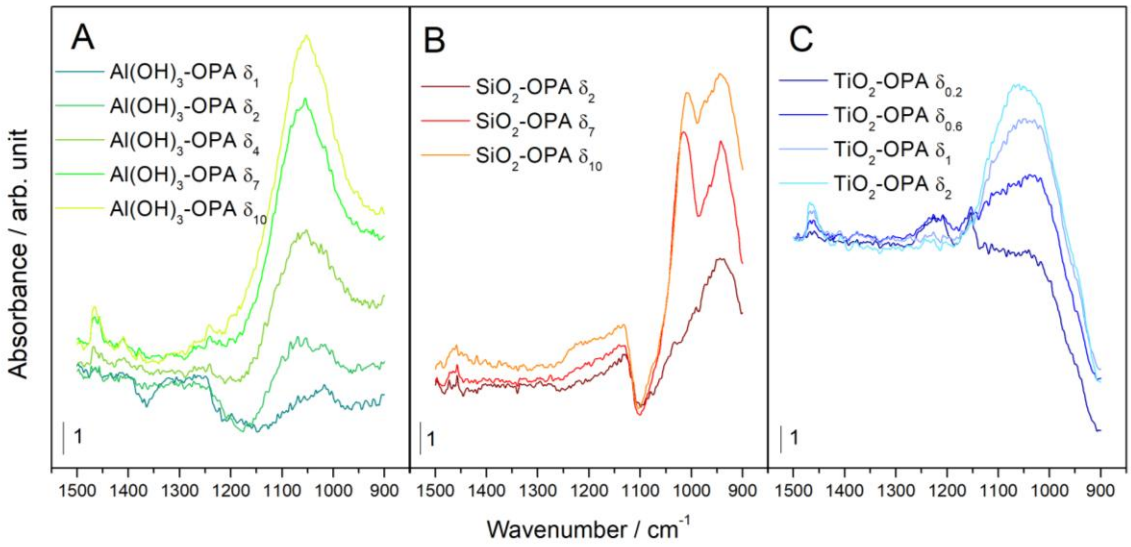
A
Al(OH)3-OPA δ1
Al(OH)3-OPA δ2
Al(OH)3-OPA δ4
Al(OH)3-OPA δ7
Al(OH)3-OPA δ10
B
SiO2-OPA δ2
SiO2-OPA δ7
SiO2-OPA δ10
C
TiO2-OPA δ0.2
TiO2-OPA δ0.6
TiO2-OPA δ1
TiO2-OPA δ2
Absorbance / arb. unit
Wavenumber / cm-1
1500 1400 1300 1200 1100 1000 900

Figure 3

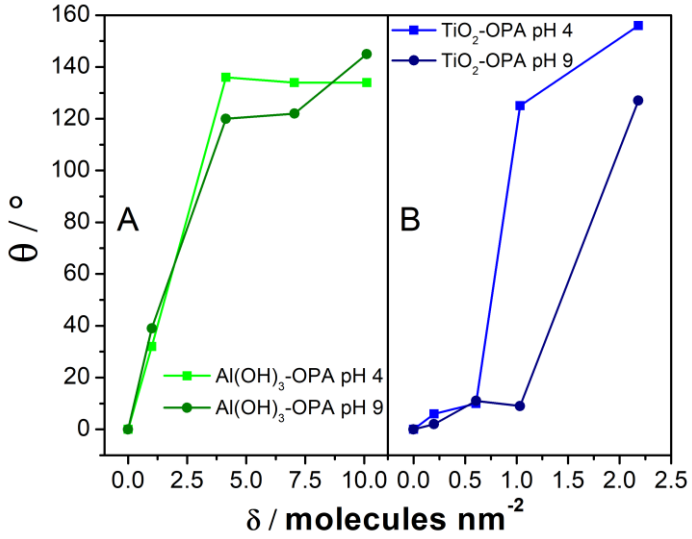
160
140
120
100
80
60
40
20
0
θ / °
A
B
Al(OH)3-OPA pH 4
Al(OH)3-OPA pH 9
TiO2-OPA pH 4
TiO2-OPA pH 9
0.0
2.5
5.0
7.5
10.0
0.0
0.5
1.0
1.5
2.0
2.5
δ / molecules nm-2

Figure 4

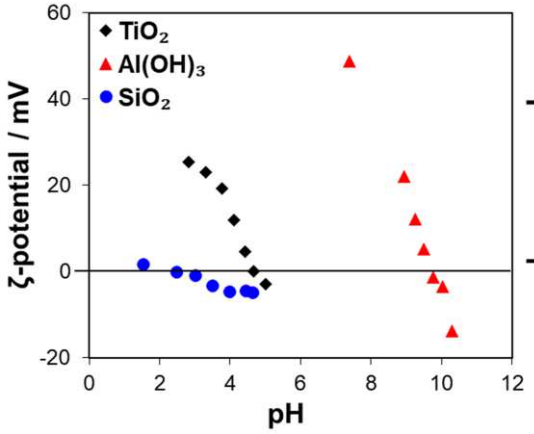

Sample	pH_{IEP}
TiO_2	4.7
$Al(OH)_3$	9.7
SiO_2	1.9

Figure 5

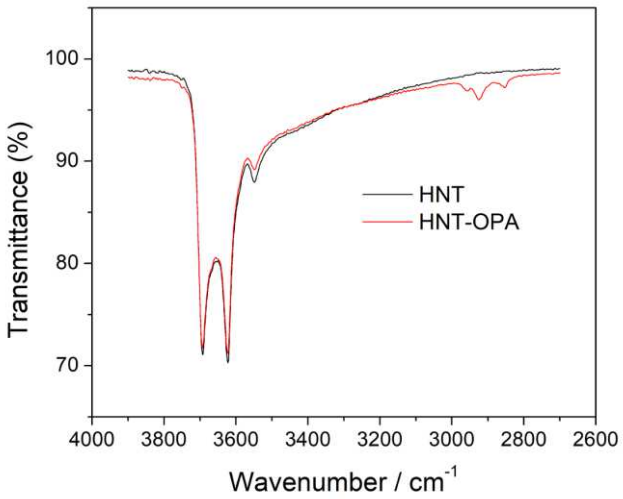
Transmittance (%)
100
90
80
70
4000
3800
3600
3400
3200
3000
2800
2600
Wavenumber / cm-1
HNT
HNT-OPA

Figure 6

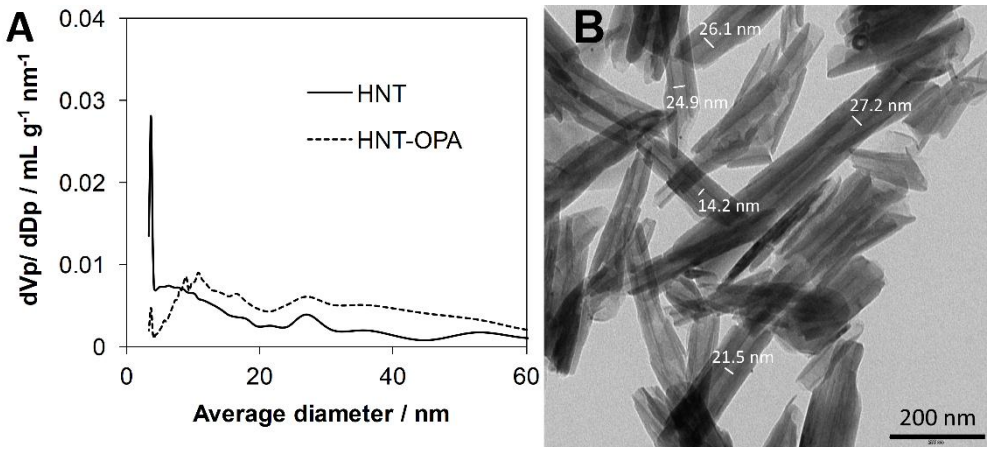
A
0.04
0.03
0.02
0.01
0
dVp/ dDp / mL g-1 nm-1
HNT
HNT-OPA
0
20
40
60
Average diameter / nm
B
26.1 nm
24.9 nm
27.2 nm
14.2 nm
21.5 nm
200 nm

Figure 7

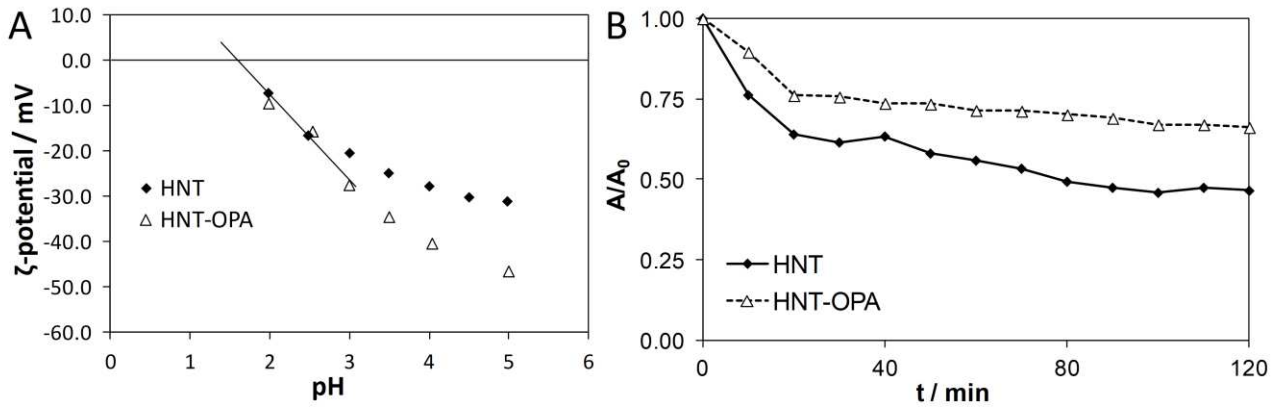
A
10.0
0.0
-10.0
-20.0
-30.0
-40.0
-50.0
-60.0
ζ-potential / mV
HNT
HNT-OPA
0
1
2
3
4
5
6
pH
B
1.00
0.75
0.50
0.25
0.00
A/A0
HNT
HNT-OPA
0
40
80
120
t / min

Figure 8

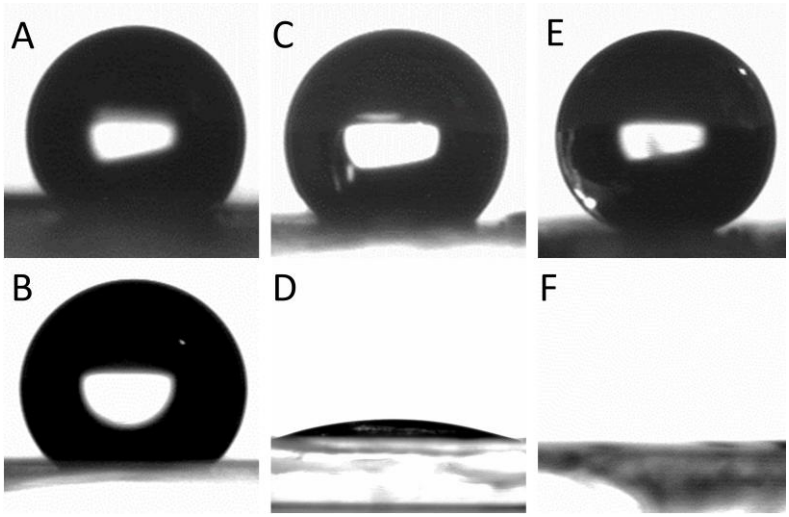

Figure 9